energies

MDPI

Article

Influence of Water Saturation, Grain Size of Quartz Sand and Hydrate-Former on the Gas Hydrate Formation

Yulia Zaripova [1], Vladimir Yarkovoi [1], Mikhail Varfolomeev [1,2,*], Rail Kadyrov [2] and Andrey Stoporev [1,2,3,4,*]

[1] Department of Physical Chemistry, Kazan Federal University, Kremlevskaya Str. 18, 420008 Kazan, Russia; yu-ya98@yandex.ru (Y.Z.); waldemaryarkovoi@gmail.com (V.Y.)
[2] Department of Petroleum Engineering, Kazan Federal University, Kremlevskaya Str. 18, 420008 Kazan, Russia; rail7777@gmail.com
[3] Nikolaev Institute of Inorganic Chemistry SB RAS, Ac. Lavrentiev Ave. 3, 630090 Novosibirsk, Russia
[4] Department of Natural Sciences, Novosibirsk State University, Pirogova Str. 1, 630090 Novosibirsk, Russia
* Correspondence: mikhail.varfolomeev@kpfu.ru (M.V.); stopor89@bk.ru (A.S.); Tel.: +7-843-233-7977 (M.V.)

Abstract: The development of technologies for the accelerated formation or decomposition of gas hydrates is an urgent topic. This will make it possible to utilize a gas, including associated petroleum one, into a hydrate state for its further use or to produce natural gas from hydrate-saturated sediments. In this work, the effect of water content in wide range (0.7–50 mass%) and the size of quartz sand particles (porous medium; <50 μm, 125–160 μm and unsifted sand) on the formation of methane and methane-propane hydrates at close conditions (subcooling value) has been studied. High-pressure differential scanning calorimetry and X-ray computed tomography techniques were employed to analyze the hydrate formation process and pore sizes, respectively. The exponential growth of water to hydrate conversion with a decrease in the water content due to the rise of water–gas surface available for hydrate formation was revealed. Sieving the quartz sand resulted in a significant increase in water to hydrate conversion (59% for original sand compared to more than 90% for sieved sand). It was supposed that water suction due to the capillary forces influences both methane and methane-propane hydrates formation as well with latent hydrate forming up to 60% either without a detectable heat flow or during the ice melting. This emphasizes the importance of being developed for water–gas (ice–gas) interface to effectively transform water into the hydrate state. In any case, the ice melting (presence of thawing water) may allow a higher conversion degree. Varying the water content and the sand grain size allows to control the degree of water to hydrate conversion and subcooling achieved before the hydrate formation. Taking into account experimental error, the equilibrium conditions of hydrates formation do not change in all studied cases. The data obtained can be useful in developing a method for obtaining hydrates under static conditions.

Keywords: gas hydrates; methane; methane-propane mixture; quartz sand; water saturation; gas storage

Citation: Zaripova, Y.; Yarkovoi, V.; Varfolomeev, M.; Kadyrov, R.; Stoporev, A. Influence of Water Saturation, Grain Size of Quartz Sand and Hydrate-Former on the Gas Hydrate Formation. *Energies* **2021**, *14*, 1272. https://doi.org/10.3390/en14051272

Academic Editor: Alexei Milkov

Received: 9 January 2021
Accepted: 19 February 2021
Published: 25 February 2021

1. Introduction

Gas hydrates have been known since the end of the 18th century. They are clathrate compounds, composed of small molecules located in the cells built by hydrogen-bonded water molecules, which can be formed under low temperature and high pressure conditions [1]. By structure, gas hydrates can be divided into three main groups, namely sI, sII and sH. Unit cell of sI hydrates is formed with 2 tetrakaidecahedron and 6 dodecahedron cavities; the unit cell consists of 46 water molecules; such a structure is characteristic of hydrates of methane, carbon dioxide, hydrogen sulfide, and ethane. sII structure consists of 16 dodecahedron and 8 hexadecahedron cavities; the unit cell contains 136 water molecules; such hydrates are formed by propane, isobutane, as well as nitrogen, oxygen, argon. Finally, unit cell of sH hydrates consists of 3 dodecahedron, 2 irregular dodecahedron and one irregular icosahedron cavities; the cell consists of 34 water molecules; sH type hydrates are

formed if heavy molecules such as 2,2-dimethylbutane, methylcyclopentane are present in a mixture of hydrocarbons. More information can be found in [2,3].

Since the beginning of the 20th century, the formation of gas hydrates in pipelines has been regarded as a serious problem for the oil and gas industry, as this process can lead to emergencies and, consequently, to a threat to human safety, huge economic losses and environmental pollution [4,5]. On the other hand, the development of gas hydrate nature-mimic technologies is important for the storage and transportation of natural gas, capture of carbon dioxide, desalination, combustion and even refrigeration processes [6–10], since one volume of hydrate can accommodate up to 160 volumes of gas [1]. Besides, hydrates are widespread in nature (up to 99% of natural gas hydrates occur in marine sediments) [11–13]. However, estimates of gas hydrate resources vary widely and generally decreased from the 1970s to the 2000s as more subsurface data became available [11]. Altogether, gas hydrates may be a future energy resource, but only where the accumulations are large and concentrated [14]. At the same time, natural gas as a fuel is much more environmentally friendly than coal and oil since it has a high calorific value; when it is burned, only carbon dioxide and water are formed [9,15]. Four main methods of gas hydrate field development have been proposed [16]: depression [17,18], heating [19,20], injection of inhibitors [21–23], and replacement with carbon dioxide [24,25]. In this regard, the study of the formation and decomposition of gas hydrates in porous media is a key point for a fundamental understanding of natural gas hydrates' behavior, the development of technologies for their extraction and practical application in the processes of transportation and storage.

A significant drawback that hinders the large-scale industrial applications of hydrates is their low formation rate. Hydrate formation can be promoted in several ways, including through the use of porous materials [26–28]. As hydrate formation is an exothermic process that proceeds at low temperatures, heat and mass transfer in the system play an important role [29,30]. The presence of a porous medium improves heat transfer conditions by increasing the thermal conductivity coefficient. Moreover, an increase in the interface area increases the nucleation rate [31]. Therefore, studies of the gas hydrates formation in porous media such as silica gel [32], activated carbon [27,32], corundum, silicon carbide [33], pumice [34], natural marine sediments [35], and clay minerals [36,37] were carried out. However, quartz sand remains the most common medium used for this purpose. Professor Linga et al. [38] studied the formation of gas hydrates in water–quartz sand system (fixed-bed column) and in bulk water (both in quiescent and stirring conditions). The results showed that the hydrate formation rate in quartz sand was much higher than in the aquatic environment. In addition, in experiments using a porous medium, a higher conversion of water to hydrate was found. It was also reported [39] that a large surface area of dispersed particles reduces the induction time of hydrate formation (of course, in the case of a developed water–gas interface).

According to the literature, particle size is one of key factors affecting the gas hydrates formation in a porous media [40,41]. It was shown [42] that media with a particle size of fewer than 4 μm are characterized by a significant shift in the equilibrium conditions of hydrate formation towards lower temperatures and higher pressure. This indicates an inhibitory effect due to both a decrease in the bound water activity and the size effect in confined pores. According to studies [43,44], the rate of hydrate formation is higher in quartz sand with smaller particles. Another relevant characteristic for hydrate formation in porous sediments is water saturation [35,40,41,45]. It was shown that an increase in water saturation resulted in a decrease in water to hydrate conversion while the addition of sodium dodecyl sulfate removing this restriction. Thus, similar systems can be promising for developing clathrate hydrate technologies for a hydrate-forming gas utilization.

Previous studies indicate that both particle size and saturation in a porous medium are important factors affecting hydrate formation. However, there is still no data on the effect of water saturation in a wide range on the formation of methane and natural gas hydrates. The aim of this research was to study the effect of water saturation on the formation and decomposition of methane and methane-propane hydrates in a porous

medium, which was taken as quartz sand with different particle sizes. High-pressure micro-differential scanning calorimetry (HP-μDSC) was employed. This technique allows one to study both thermodynamic and kinetic features of the gas hydrates formation and dissociation processes [46–48].

2. Materials and Methods

Methane with a purity of 99.95% was used for methane hydrates formation experiments. To study the formation of natural gas hydrates, a model gas mixture containing 9.1 mol% propane and 90.9 mol% methane was used. Quartz sand and deionized water were employed as hydrate-forming medium.

The analysis of the granulometric composition of quartz sand was carried out on a vibrating sieve from Fritsch (Germany). The device includes a set of sieves ranging in size from 1 mm to 0.025 mm. To analyze the granulometric composition, a prepared sample with a known mass was poured into a stack of sieves of different dimensions (sieves are located from top to bottom from larger to smaller). Then, the lid of the device was closed, and the program was set to vibration for 10 min with an amplitude of 2 mm. After 10 min, the weight of the sample fraction deposited on each sieve was measured. X-ray computed microtomography (CT) was used as well (General Electric V | TOME | X S 240 tomograph, Germany). The resolution was 1.5 μm. Avizo 7.1. software was employed to build the virtual models of porous structure.

To study the processes of formation and dissociation of gas hydrates in a porous medium and the influence of various factors on these processes, a number of experiments were carried out using high-pressure micro-differential scanning calorimeter HP-μDSC 7 Evo (Setaram Instrumentation, France). The calorimeter is equipped with a three-dimensional Calvet sensor that allows the total heat flux to be recorded. The operating temperature range is from −45 °C to 120 °C. The programmable rate of temperature change can vary from 0.001 to 2 °C/min. A high-pressure cell capable of withstanding pressures up to 40 MPa was taken. The maximum difference between the repeated measurements for the same system did not exceed 0.8 °C and 1% for temperature and heat effect, respectively.

The experimental technique was as follows. The cell was filled with deionized water and quartz sand in a certain weight ratio (from 1:1 to 1:100) so that the total weight of the system did not exceed 150 mg, stirred and sealed. The pressure was injected using the gas panel, 9 MPa in the case of methane, 2.2 MPa in the case of a gas mixture. The cell was placed in the calorimeter and, after the signal stabilized, the experiment was started.

Temperature program in the case of studying methane hydrates: the isotherm was maintained at 20 °C for 10 min, then the sample was cooled to −35 °C at a rate of 0.25 °C/min, after which it was heated to 20 °C at a rate of 0.25 °C/min, the cycle was repeated 3 times. Temperature program in the case of studying hydrates of a methane-propane mixture: an isotherm was maintained at 30 °C for 10 min, then the sample was cooled to −15 °C at a rate of 0.25 °C/min, and then heated to 30 °C at a rate of 0.25 °C/min, the cycle was repeated 3 times. The values of temperatures and heat effects of the recorded phase transitions were found using the Calisto Processing software.

3. Results

3.1. Granulometric Analysis

To study the effect of water saturation on the formation of methane and methane-propane mixture hydrates, original quartz sand (O) as well as its small (S) and medium (M) fractions were used. The particle size distribution was determined by X-ray CT. The average particle size of original quartz sand was also analyzed by sieving. The results are shown in Figure 1 and Table 1.

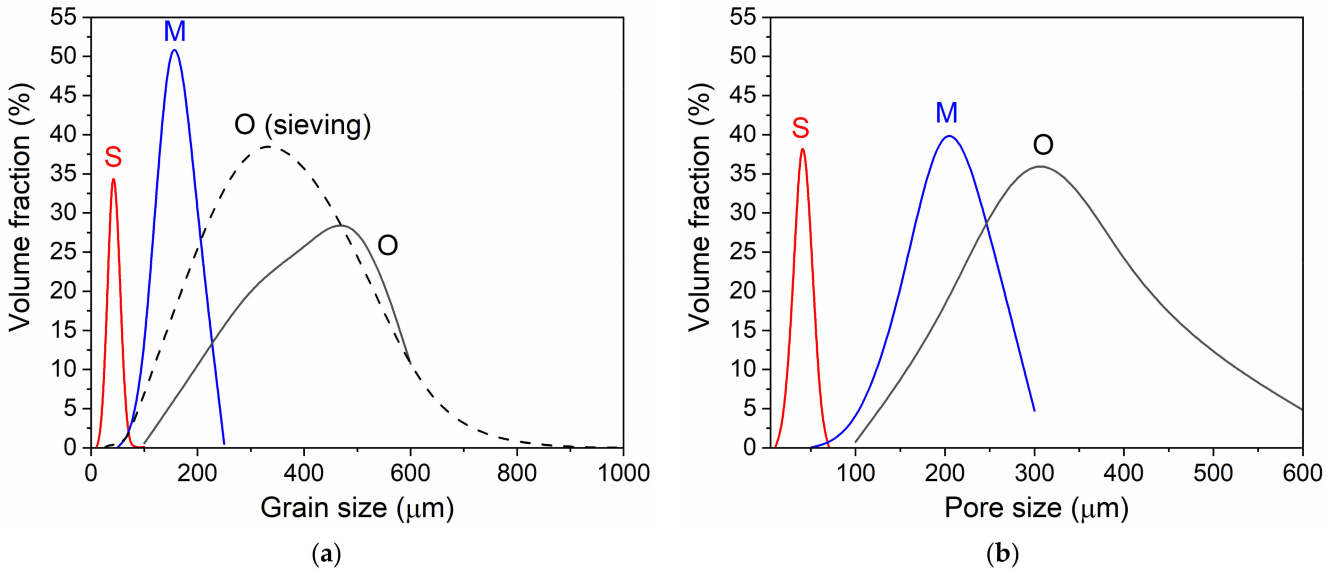

(**a**) (**b**)

Figure 1. (**a**) Grain and (**b**) pore size distributions of quartz sand determined by sieving (dash line) and X-ray CT (solid lines); S and M are small and medium fractions, O corresponds to original sand.

Table 1. Characteristics of the used fractions of quartz sand.

Quartz Sand Fractions	Grain Size by Sieving (μm)	Grain Size by CT/Mean Size (μm)	Mean Pore Size by CT (μm)	Porosity (φ)
Small (S)	< 50	10–80/43.3 ± 0.5	41.5 ± 0.6	0.34
Medium (M)	125–160	50–250/162 ± 2	208 ± 2	0.46
Original unsifted sand (O)	30–800	100–600/460 ± 80	320 ± 10	0.41

The pore network models built according to the algorithm described in [49] is presented in Figure 2.

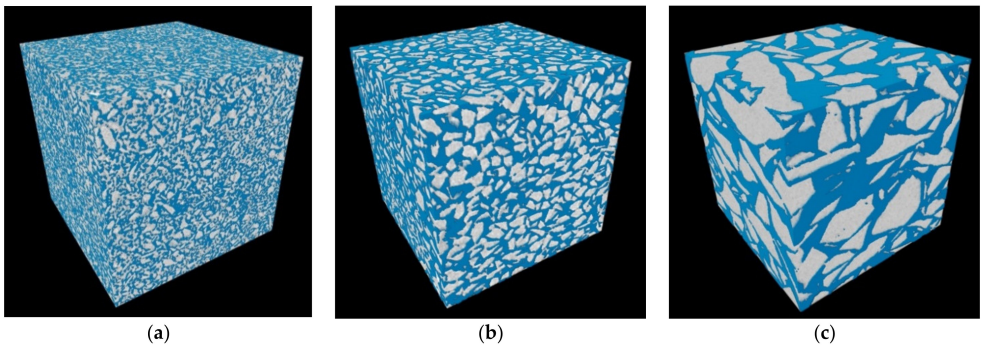

(**a**) (**b**) (**c**)

Figure 2. 3D visualization of pore structure for (**a**) S fraction, (**b**) M fraction, and (**c**) original unsifted sand O with sand grains in gray and pore volume in blue.

3.2. Influence of Water Saturation on the Methane Hydrate Formation

As already noted, the method of high-pressure differential scanning calorimetry allows one to determine the thermodynamic characteristics of the processes of formation and decomposition of gas hydrates. Figure 3 shows a typical DSC-curve of the formation/dissociation of hydrate and ice upon successive cooling and heating.

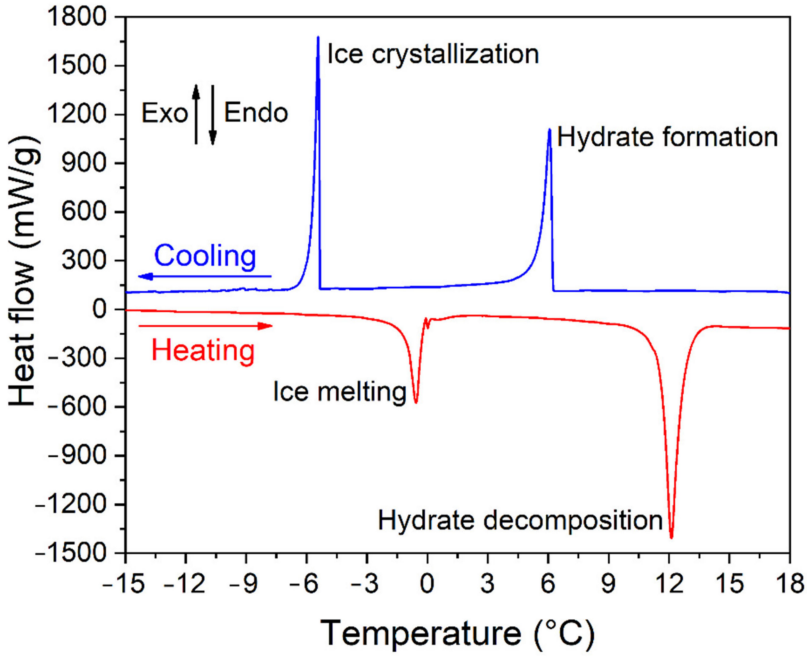

Figure 3. Typical DSC curve for the methane—water—sand system under pressure of 9 MPa; water:sand mass ratio is 1:50; cooling/heating rate equals to 0.25 °C/min; heat flow is normalized to water content.

At the first stage of the work, the effect of water saturation of quartz sand on the formation of methane hydrates was investigated. Samples with different ratio of water to sand (by weight) equaled to 1:1, 1:2, 1:4, 1:6, 1:8, 1:10, 1:15, 1:20, 1:50, 1:100 were used for the experiments. Table 2 presents the obtained values of temperature and heat effect of methane hydrate/ice formation and melting/decomposition.

Table 2. Values of temperature and heat effect (enthalpy ΔH) for the ice and methane hydrate formation and melting/decomposition at different water saturation (WS) of studied samples; T_{eq} is equilibrium temperature of hydrate decomposition.

m_w/m_s	WS	Content of O Sand (Mass%)	$\Delta H_{ice\ cryst}$ (J/g) [1]	$\Delta H_{ice\ melt}$ (J/g) [1]	$T_{hyd\ onset}$ (°C)	$\Delta H_{hyd\ form}$ (J/g) [1]	T_{eq} (°C)	$\Delta H_{hyd\ dec}$ (J/g) [1]
1:1	3.74	50.0	−299 ± 4	323 ± 3	–	–	11.0	16 ± 3
1:2	1.87	66.7	−327 ± 4	333 ± 4	−7.4 ± 0.1	−2.3 ± 0.1	11.5	28 ± 3
1:4	0.94	80.0	−317 ± 19	306 ± 7	0.5 ± 5	−15.7 ± 0.1	12.0	68 ± 9
1:6	0.62	85.7	−310 ± 7	312 ± 3	−3 ± 2	−19 ± 4	11.2	74 ± 5
1:8	0.47	88.9	−320 ± 23	312 ± 3	2.3 ± 0.8	−33 ± 2	11.8	121 ± 17
1:10	0.37	90.9	−287 ± 41	255 ± 5	−2 ± 2	−54 ± 13	11.3	167 ± 2
1:15	0.25	93.8	−329 ± 1	275 ± 4	–	–	11.8	192 ± 15
1:20	0.19	95.2	−219 ± 26	206 ± 18	5 ± 6	−99 ± 24	11.9	212 ± 9
1:50	0.07	98.0	−151 ± 48	111 ± 10	4 ± 6	−145 ± 25	11.9	296 ± 10
1:100	0.04	99.0	−113 ± 30	66 ± 17	3 ± 5	−177 ± 32	11.9	308 ± 14

[1] Normalized per water content.

Water saturation (WS) of the sand was calculated as follows.

$$WS = V_w/V_p = \rho_s\ m_w\ (1\text{-}\varphi)/\rho_w\ \varphi\ m_s, \quad (1)$$

where V_w and V_p are water and pore volumes, ρ_s and ρ_w are the sand and water densities (2.6 and 1 g/cm^3, respectively), m_w/m_s corresponds to water:sand mass ratio, and φ is the porosity.

3.3. Influence of Water Saturation on the Formation of Methane-Propane Hydrate

At the second stage, the effect of water saturation of quartz sand on the formation of hydrates of a gas mixture consisting of methane and propane was studied at a pressure of 2.2 MPa. On the one hand, this pressure was chosen in order to avoid condensation of the mixture, and, on the other hand, to carry out measurements with the same driving force for methane hydrates and methane-propane mixture, since the equilibrium temperature of hydrate formation in this case is 12.2 °C. For the experiments, we used systems with a water:sand ratio (by mass) of 1:1, 1:4, 1:10, 1:100. The results are shown in Table 3.

Table 3. Values of temperature and heat effect (enthalpy ΔH) for the ice and methane-propane hydrate formation and melting/decomposition at different water saturation (WS) of studied samples; T_{eq} is equilibrium temperature of hydrate decomposition.

WS	Content of O Sand (Mass%)	$\Delta H_{ice\ cryst}$ (J/g) [1]	$\Delta H_{ice\ melt}$ (J/g) [1]	$T_{hyd\ onset}$ (°C)	$\Delta H_{hyd\ form}$ (J/g) [1]	T_{eq} (°C)	$\Delta H_{hyd\ dec}$ (J/g) [1]
3.74	50.0	325 ± 3	349 ± 3	–	–	12.3	7.8 ± 0.6
0.94	80.0	358 ± 3 [2]	310 ± 7	−4.9 ± 0.2	358 ± 3 [2]	11.0	65 ± 11
0.37	90.9	408 ± 44 [2]	120 ± 43	−4.6 ± 0.1	408 ± 44 [2]	11.4	407 ± 74
0.04	99.0	–	6 ± 6	0 ± 5	470 ± 32	10.8	449 ± 6

[1] Normalized per water content. [2] Simultaneous ice + hydrate formation.

3.4. Influence of the Size of Quartz Sand Particles on the Formation of Methane Hydrates

We also examined the effect of the size of quartz sand particles on the formation of methane hydrate. Fractions with a particle size of less than 0.05 mm and from 0.125 to 0.16 mm were separated using a sieve system. The mass fraction of sand for these experiments was 96.8% (1:30 water to sand ratio). This ratio was chosen based on the data on the heat effect of hydrate decomposition (compare the data in Tables 2 and 4 for O sand). Indeed, at a ratio of 1:30, the heat effect of hydrate decomposition normalized to the water content is the same as for a ratio of 1:50 at a higher water content. An additional sample was also prepared by water vapor sorption. A sample of sand S was placed in a desiccator over deionized water and kept for up to a month. This provided an even distribution of water in the pore space of the sand. In the case of a sample of 1:100, the water content is close, however, with mechanical mixing of water and sand, we cannot say that the water was evenly distributed over the sample. In this case, different weights of the sample were taken in order to check whether the sensitivity of the instruments is sufficient for a quantitative characterization of the occurring processes. The results of DSC studies are shown in Table 4.

Table 4. Values of temperature and heat effect (enthalpy ΔH) for the ice and methane-propane hydrate formation and melting/decomposition; T_{eq} is equilibrium temperature of hydrate decomposition depending on the particle size of quartz sand; water-sand ratio is 1:30 (96.8% of sand by mass).

Quartz Sand Fraction	WS	$\Delta H_{ice\ cryst}$ (J/g) [1]	$\Delta H_{ice\ melt}$ (J/g) [1]	$T_{hyd\ onset}$ (°C)	$\Delta H_{hyd\ form}$ (J/g) [1]	T_{eq} (°C)	$\Delta H_{hyd\ dec}$ (J/g) [1]
S	0.17	−145 ± 52	148 ± 35	1 ± 5	−318 ± 53	11.3	459 ± 13
M	0.10	–	5.0 ± 0.8	5 ± 7	−445 ± 2	11.8	447 ± 4
O	0.12	−320 ± 46	256 ± 11	0.3 [2]	−95.5 [2]	11.9	296 ± 16
S [3]	0.04	–	–	−6 ± 3	−159 ± 23	10.6	138 ± 4
S [4]		–	–	−7 ± 3	−105 ± 4	11.0	105 ± 1

[1] Normalized per water content. [2] Hydrate occurred only in the 3rd cycle. [3] Sample was prepared by water sorption (withstanding of S fraction in water vapor atmosphere above the deionized water in a desiccator); 1:136 water to sand ratio (99.3 mass% of sand); full DSC cell loading (311.83 mg). [4] Sample was prepared by water sorption (withstanding of S fraction in water vapor atmosphere above the deionized water in a desiccator); 1:136 water to sand ratio (99.3 mass% of sand); half DSC cell loading (148.92 mg).

4. Discussion

Influence of Water Saturation, Grain Size of Quartz Sand and Hydrate-Former on Gas Hydrate Formation

The equilibrium temperature of hydrate formation for methane hydrate at 9 MPa, as well as for methane-propane hydrate at 2.2 MPa, calculated with the CSM Gem software [1] is about 12 °C. Thus, formation of the methane (sI type) and methane-propane (sII type) hydrates was studied at the same conditions (subcoolings). It was observed that the presence of a porous medium does not shift the equilibrium conditions of the hydrate phase existence within experimental error (Figure 4). This can be explained by a sufficiently large sand grain and pore size.

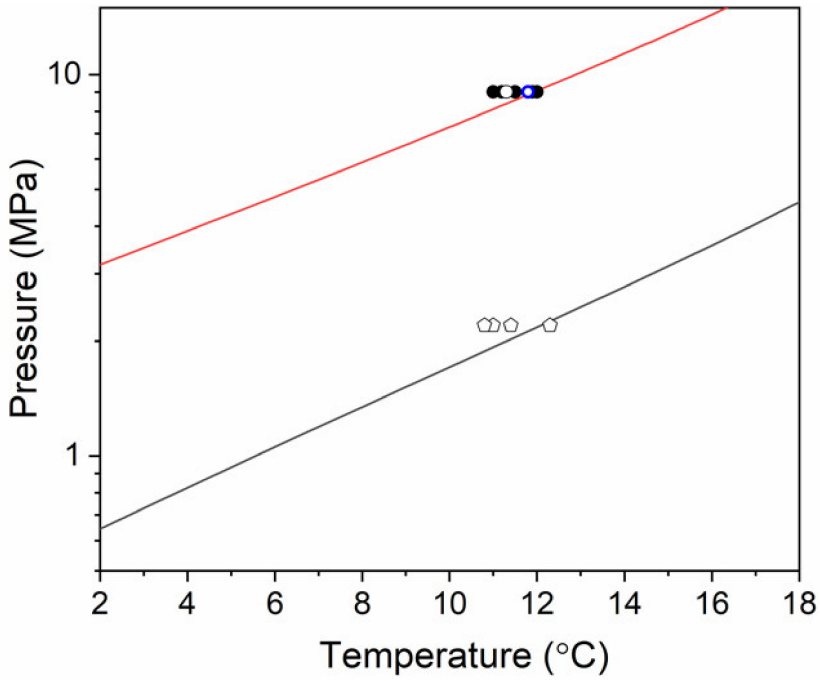

Figure 4. Equilibrium conditions of a hydrate formations in the studied systems: red and black lines correspond to the calculated gas–hydrate–water equilibrium curves for methane and methane-propane mixture, respectively (CSM Gem software [1]); different symbols denote experimental temperature of a hydrate decomposition at 9 and 2.2 MPa for methane and methane-propane mixture, respectively (see Tables 2 and 3).

Figure 5a shows the dependence of the hydrate onset temperature on the number of the cooling/heating cycle. An increase in the temperature of hydrate formation from cycle to cycle was frequently observed. This could be due to memory effect. It is possible that in the first cycle supersaturation is created because of gas bubbles, which persists for some time [50,51]. Despite the fact that weighed water and sand were thoroughly mixed in the cell before gas supply, another reason may be an increase in the water–gas contact surface due to the redistribution of water after the cycle of hydrate formation and decomposition. Conducting a larger number of cycles is necessary to determine the stability of the system and clarify the reasons for the decrease in subcooling of hydrate formation achieved in subsequent cycles. Elucidation of the stability in time of the possible aqueous phase supersaturation with a gas is also the subject of a separate work. In any case, this feature is useful for the implementation of hydrate formation in such systems. It should be noted that the pore space is completely filled with water at high WS (greater than 1). A gas hydrate seems to be formed only on the sample surface. In this case, there is no developed water–gas contact surface available for an enhanced hydrate formation like at low WS (smaller than 1). As can be seen from Figure 5b, a decrease in WS increases

the temperature of hydrate formation except of the S fraction sample with adsorbed water. This result supports the concept that the developed water–gas surface facilitates the hydrate formation.

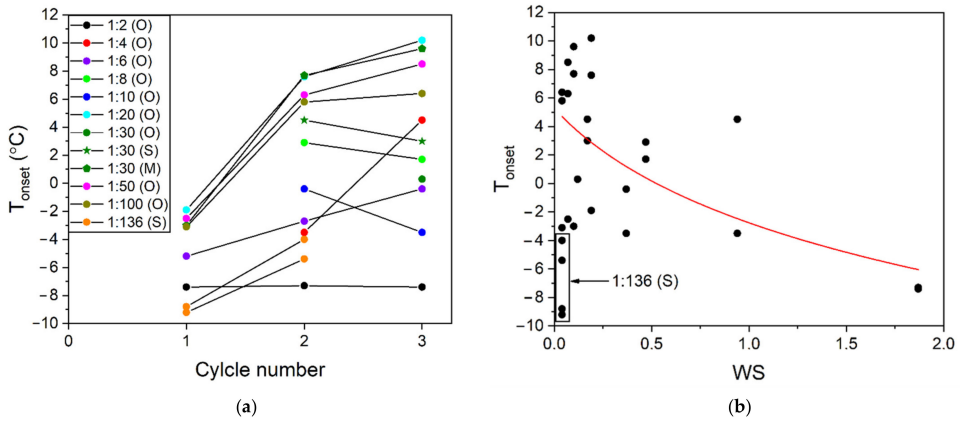

Figure 5. Methane hydrate onset temperature vs. (**a**) the cycle number (sand fractions are in the figure) and (**b**) water saturation.

In the case of a sample with a water-to-sand ratio of 1: 136 obtained by sorption of water vapor, the hydrate was formed at higher supercooling. This can be related to the distribution of unrelated microvolumes of water in the pore space. In this case, the formation of hydrate in such volume may not be detected by the DSC device. As a result, the apparent formation of hydrate is recorded when a certain critical subcooling is reached.

The heat effect of hydrate decomposition per gram of water increases with a decrease in the particle size (Figure 6). This is apparently due to an increase in the interface, which once again confirms the results of previous studies [31,40,52].

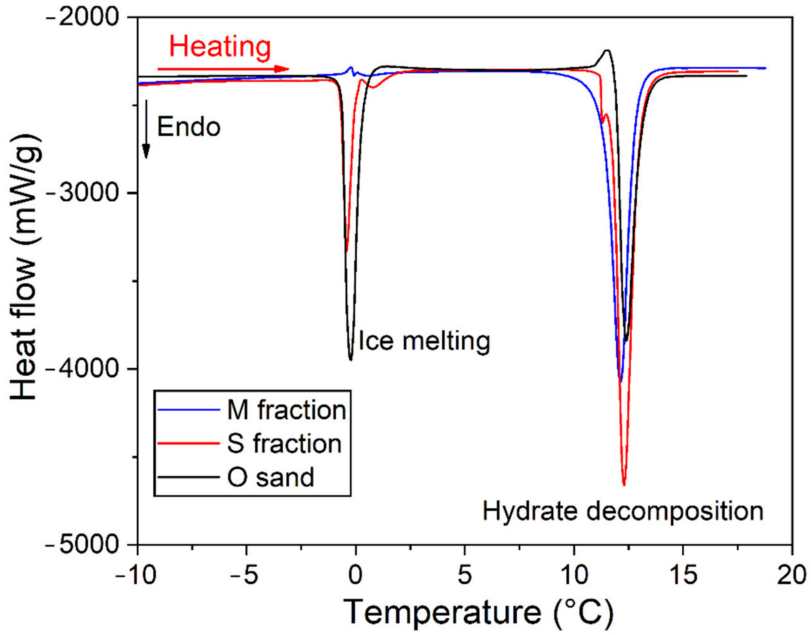

Figure 6. Effect of the grain size of quartz sand on the formation of methane hydrate; average decomposition curves are shown.

It can be noted that ice crystallization was observed in the system with sand O and S, while this was almost undetectable with sand M (Figure 6 and Table 4). Such a latent crystallization can take place if microvolumes of water are separated from each other [53].

The pores in M fraction are bigger compared to the S one, so that the WS is lower for M fraction at the same water content that can lead to the isolation of water microvolumes making a quite uniform water distribution in the sample which readily affects nucleation and further growth of gas hydrates. In the case of a sample with sand S with adsorbed water, ice also did not crystallize (or we did not record this because of a too small heat flow). In the latter case, this can be explained by a small volume of water at a high water–gas contact area which facilitate the formation of hydrate (surface-dependent process) compared to ice. At the same time, additional formation of hydrate was observed after ice melting in the sample of unsifted sand. Figure 7 shows the dependence of the amount of such a reformed hydrate on the composition of the system. It is clear that this process is also triggered by the presence of a developed contact of water with hydrate-forming gas. It seems that the thawing water–gas surface area to water volume ratio is maximal at 0.25 WS and starts to decrease with a WS increase resulting in a decrease in water available for the reformation process.

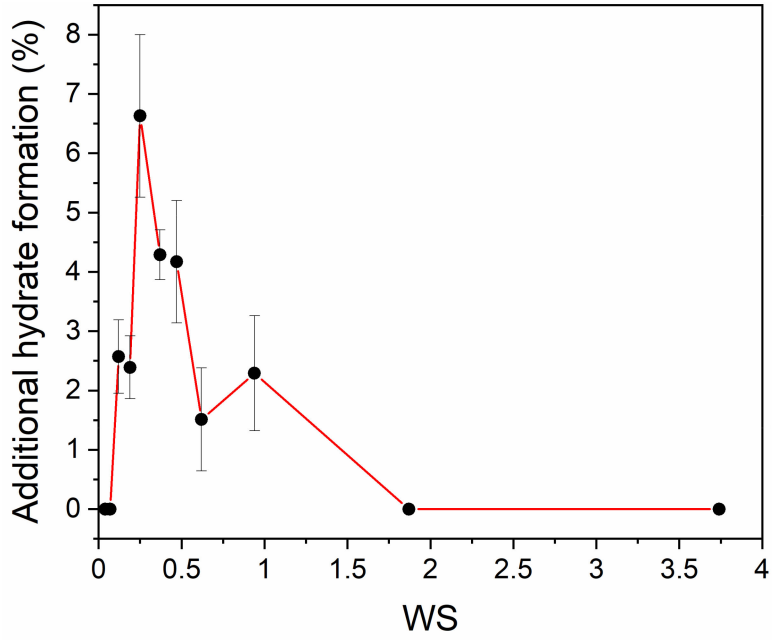

Figure 7. Effect of the water saturation on the hydrate reformation process.

Thus, the thermal effect of hydrate decomposition normalized to the mass of water in the system increases with a decrease in water saturation, while the heat effect of ice melting decreases (Tables 2 and 3). The conversion of water to hydrate in a system was calculated as follows:

$$\omega = 100^{*}\Delta H/\lambda, \quad (2)$$

where ω is the mass percentage of the water transformed to hydrate, ΔH is the enthalpy of hydrate decomposition expressed in J/g, and λ is the specific heat of a hydrate decomposition. For methane hydrate λ equals to 501.4 J per gram of water [1] for $CH_4 \cdot 6H_2O$ hydrate composition [1,54]. Calculation in CSM Gem showed that at 12 °C and 2.2 MPa the equilibrium composition of the methane-propane hydrate is $1.6CH_4 \cdot C_3H_8 \cdot 17.5H_2O$ or $G \cdot 6.9H_2O$ (G—guest). In this case, the enthalpy of decomposition of the hydrate into gas and water, calculated per gram of water, is 637.2 J/g. Obtained results are presented in Table 5.

Table 5. Conversion of water into a hydrate at different water saturation of quartz sand.

Sand Type	m_w/m_s	WS	Water to Hydrate Conversion of (%)
Methane hydrate			
O	1:1	3.74	3 ± 1
	1:2	1.87	6 ± 1
	1:4	0.94	14 ± 2
	1:6	0.62	15 ± 1
	1:8	0.47	24 ± 3
	1:10	0.37	33 ± 1
	1:15	0.25	38 ± 3
	1:20	0.19	42 ± 2
	1:50	0.07	59 ± 2
	1:100	0.04	61 ± 3
Methane hydrate; different sand fractions			
O	1:30	0.12	59 ± 3
S		0.17	92 ± 3
M		0.10	89 ± 1
S	1:136	0.04	28 ± 1 [1] 20.9 ± 0.2 [2]
Methane-propane hydrate			
O	1:1	3.74	1.2 ± 0.1
	1:4	0.94	10 ± 2
	1:10	0.37	64 ± 12
	1:100	0.04	70 ± 1

[1] For full DSC cell loading (311.83 mg; see Table 4). [2] For half DSC cell loading (148.92 mg; see Table 4).

The effect of system composition on the water to hydrate conversion is shown in Figure 8. The gas type (hydrate type in the case study) unexpectedly does not affect the conversion. However, the level of conversion differs significantly at the stage of formation (cooling). Figure 9 shows the dependence of the amount of ice on hydrate formation during the cooling stage. There is a reciprocal correlation (Figure 9; the straight lines here correspond to the linearization of the experimental data). Within the experimental error, the correlation shows that all water (100%) is transformed into ice if a hydrate does not occur. At the same time, achieving a certain degree of water transformation into hydrate, ice would not form. Surprisingly, this level of water to hydrate conversion turned out to be different depending on sand fraction (O, S, M) and gas type. The data obtained revealed that the hydrate formation in the wet sand can be tuned by proper choice of the porous medium.

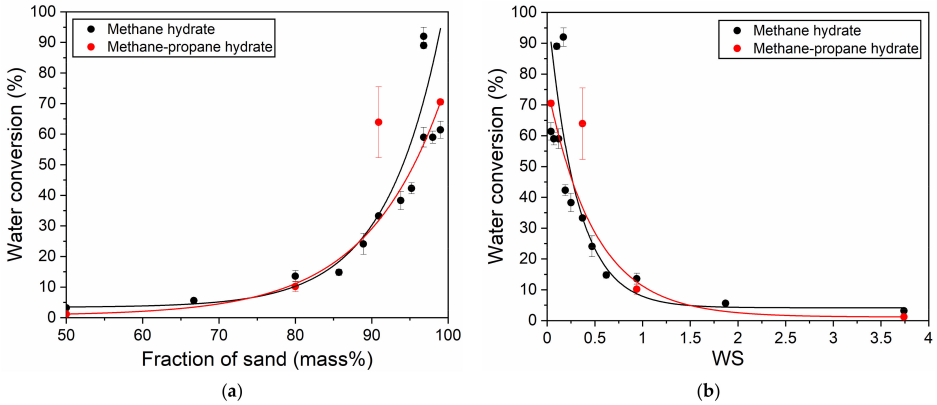

Figure 8. (**a**) Effect of the mass fraction of the porous medium on the overall water conversion (decomposition data); (**b**) effect of the water saturation on the overall water conversion (decomposition data); exponential trends are shown with solid lines.

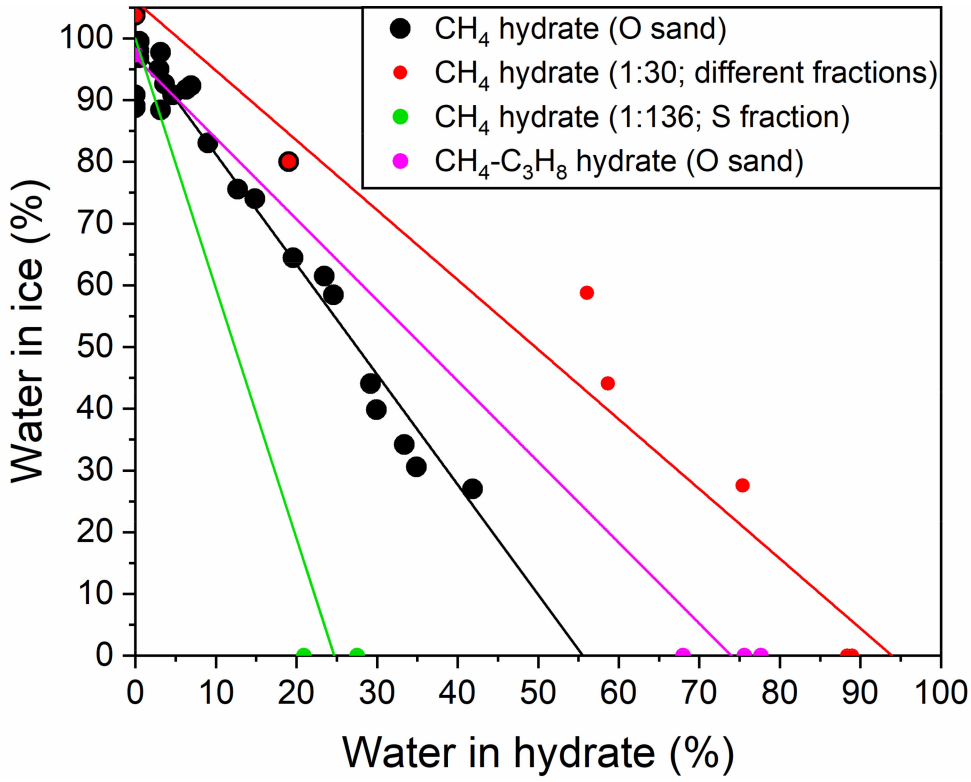

Figure 9. The dependence of water part converted into ice vs. water part transformed into hydrate (formation data).

It should be noted that in the absence of one of the solid phases (ice or hydrate), the enthalpy of melting/decomposition of the formed phase coincides well with the enthalpy of its formation (Tables 2–4 and Figure 10). In this case, some outgrowth of a hydrate from ice is always observed either in a latent form at temperatures below the ice melting point or during its melting. This process increases the gas content of the sample.

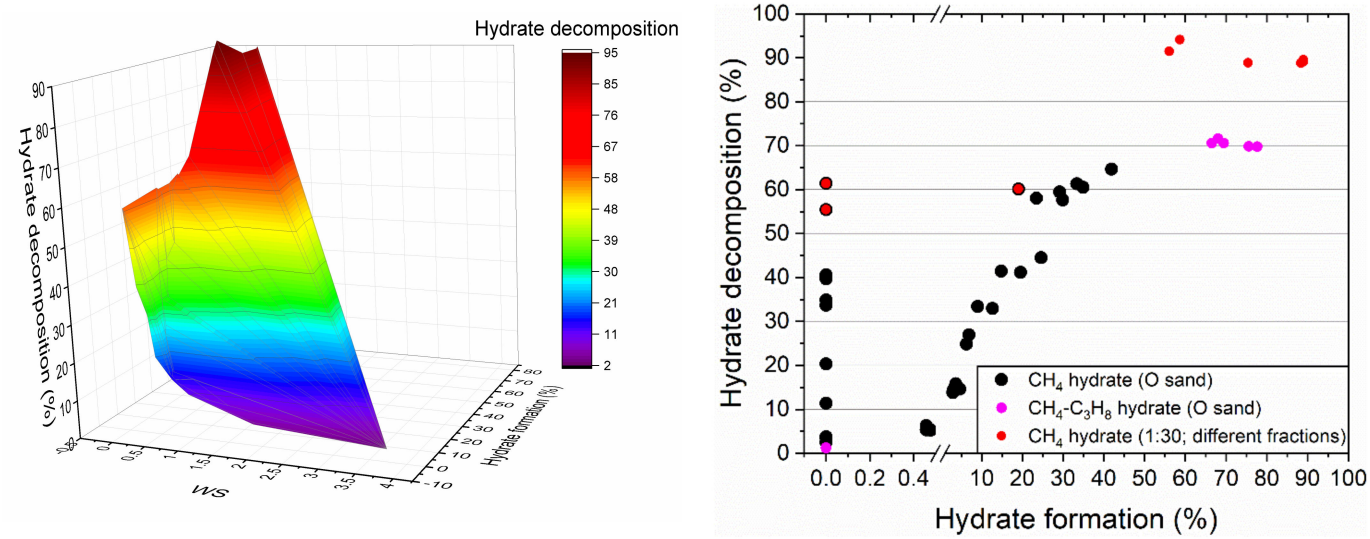

(**a**) (**b**)

Figure 10. (**a**) Influence of the WS (*X*-axis) and part of hydrate formed (*Y*-axis) on the overall water to hydrate conversion (decomposed hydrate; *Z*-axis); (**b**) Y-Z projection of the mentioned dependence.

One can see that with a decrease in the WS, the conversion of water increases significantly (Figure 10). The dependance can be divided into two branches, namely the hydrate formation from ice/melting water at initial zero and non-zero content of the hydrate after the cooling stage. At the same time, the steepness of the slope of the curve decreases (Figure 10b), which may indicate the reaching of limiting conversion value for a given sand grain size; however, this issue requires further research.

5. Conclusions

The effect of water saturation in a wide range, the size of quartz sand particles, and hydrate-forming gas (methane and methane-propane mixture) on the hydrate formation using high-pressure differential scanning calorimetry has been investigated. It was shown that the equilibrium temperature of hydrate formation does not change within the experimental error. Both sI methane and sII gas mixture hydrates demonstrate a similar increase in the conversion of water to hydrate with a decrease in the water saturation of the porous medium. The possible explanation is that the hydrate formation proceeds on the surface more intensively than in the water column due to an enhanced water–gas and/or thawing water–gas interface at a lower water saturation level with the sand polydispersity affecting both the hydrate onset temperature and conversion degree. Indeed, in the case of a sieved sand, the more uniform quartz particles packing results in more uniform water distribution in the sample (an increased water–gas interface at low water saturation), which readily affects nucleation and further growth of gas hydrates. The results obtained reveal how to optimize the composition of the hydrate production system (sand particle size and water content). The observed increase in the temperature of hydrate formation from cycle to cycle can be associated with both the memory effect and an increase in the water–gas contact surface due to the redistribution of water after hydrate formation-decomposition. It is worth noting that there is almost no difference between methane and methane-propane hydrates formation (conversion degree) at low water content. It seems to be that mass transfer limitation becomes negligible in this case. This makes it possible to avoid severe subcooling during the initialization of hydrate formation and consider similar systems as promising for developing clathrate hydrate gas utilization technologies, since it is relatively easy to implement. As the polydispersity of the sand medium and water–gas interface play an important role in the hydrate formation regardless the hydrate structure type

(for hydrocarbons), it is a relevant issue to find a way to modify the porous medium for an enhanced hydrate formation.

Author Contributions: Conceptualization, Y.Z., M.V. and A.S.; methodology, Y.Z. and A.S.; validation, Y.Z. and A.S.; data curation, Y.Z. and A.S.; writing—original draft preparation, Y.Z. and A.S.; writing—review and editing, M.V. and A.S.; formal analysis, Y.Z., M.V. and A.S.; investigation, Y.Z., V.Y. and R.K.; resources, M.V.; visualization, Y.Z. and A.S.; supervision, M.V. and A.S.; project administration, Y.Z. and A.S.; funding acquisition, M.V. All authors have read and agreed to the published version of the manuscript.

Funding: This research was funded by the subsidy allocated to Kazan Federal University for the state assignment in the sphere of scientific activities (Project №. 0671-2020-0048 of State Assignment №. 075-00216-20-05 of 04.06.2020 (Part II Section I)). Additionally, Y.Z., V.Y., M.V., A.S. acknowledge the support from RFBR and The Research Council of Norway (research project № 20-55-20010).

Institutional Review Board Statement: Not applicable.

Informed Consent Statement: Not applicable.

Data Availability Statement: The data are available from the authors.

Conflicts of Interest: The authors declare no conflict of interest.

References

1. Sloan, E.D.; Koh, C.A. *Clathrate Hydrates of Natural Gases*, 3rd ed.; CRC Press: Boca Raton, FL, USA; London, UK; New York, NY, USA, 2008.
2. Kirov, M. Atlas of optimal proton configurations of water clusters in the form of gas hydrate cavities. *J. Struct. Chem.* **2002**, *43*, 790–797. [CrossRef]
3. Manakov, A.Y.; Kosyakov, V.I.; Solodovnikov, S.F. Structural Chemistry of Clathrate Hydrates and Related Compounds. In *Comprehensive Supramolecular Chemistry II*; JL, A., Ed.; Elsevier: Oxford, UK, 2017; pp. 161–206.
4. Sloan, E.D. *Natural Gas Hydrates in Flow Assurance*; Gulf Professional Publishing: Houston, TX, USA, 2010.
5. Boswell, R.; Collett, T.S. Current perspectives on gas hydrate resources. *Energy Environ. Sci.* **2011**, *4*, 1206–1215. [CrossRef]
6. Mimachi, H.; Takeya, S.; Yoneyama, A.; Hyodo, K.; Takeda, T.; Gotoh, Y.; Murayama, T. Natural gas storage and transportation within gas hydrate of smaller particle: Size dependence of self-preservation phenomenon of natural gas hydrate. *Chem. Eng. Sci.* **2014**, *118*, 208–213. [CrossRef]
7. Babu, P.; Nambiar, A.; He, T.; Karimi, I.A.; Lee, J.D.; Englezos, P.; Linga, P. A Review of Clathrate Hydrate Based Desalination To Strengthen Energy-Water Nexus. *ACS Sustain. Chem. Eng.* **2018**, *6*, 8093–8107. [CrossRef]
8. Misyura, S. Dissociation of various gas hydrates (methane hydrate, double gas hydrates of methane-propane and methane-isopropanol) during combustion: Assessing the combustion efficiency. *Energy* **2020**, *206*, 118120. [CrossRef]
9. Misyura, S. Developing the environmentally friendly technologies of combustion of gas hydrates. Reducing harmful emissions during combustion. *Environ. Pollut.* **2020**, *265*, 114871. [CrossRef]
10. Delahaye, A.; Fournaison, L.; Dalmazzone, D. Use of Hydrates for Cold Storage and Distribution in Refrigeration and Air-Conditioning Applications. In *Gas Hydrates 2: Geoscience Issues and Potential Industrial Applications*; Wiley: Hoboken, NJ, USA, 2018; pp. 315–358. [CrossRef]
11. Milkov, A.V. Global estimates of hydrate-bound gas in marine sediments: How much is really out there? *Earth Sci. Rev.* **2004**, *66*, 183–197. [CrossRef]
12. Ruppel, C. Permafrost-Associated Gas Hydrate: Is It Really Approximately 1 % of the Global System? *J. Chem. Eng. Data* **2015**, *60*, 429–436. [CrossRef]
13. Chong, Z.R.; Yang, S.H.B.; Babu, P.; Linga, P.; Li, X.-S. Review of natural gas hydrates as an energy resource: Prospects and challenges. *Appl. Energy* **2016**, *162*, 1633–1652. [CrossRef]
14. Milkov, A.V.; Sassen, R. Economic geology of offshore gas hydrate accumulations and provinces. *Mar. Pet. Geol.* **2002**, *19*, 1–11. [CrossRef]
15. Misyura, S.Y. Non-stationary combustion of natural and artificial methane hydrate at heterogeneous dissociation. *Energy* **2019**, *181*, 589–602. [CrossRef]
16. Cui, Y.; Lu, C.; Wu, M.; Peng, Y.; Yao, Y.; Luo, W. Review of exploration and production technology of natural gas hydrate. *Adv. Geo-Energy Res.* **2018**, *2*, 53–62. [CrossRef]
17. Yang, X.; Sun, C.-Y.; Su, K.-H.; Yuan, Q.; Li, Q.-P.; Chen, G.-J. A three-dimensional study on the formation and dissociation of methane hydrate in porous sediment by depressurization. *Energy Convers. Manag.* **2012**, *56*, 1–7. [CrossRef]
18. Gao, Q.; Yin, Z.; Zhao, J.; Yang, D.; Linga, P. Tuning the fluid production behaviour of hydrate-bearing sediments by multi-stage depressurization. *Chem. Eng. J.* **2021**, *406*, 127174. [CrossRef]

19. Feng, J.-C.; Wang, Y.; Li, X.-S.; Chen, Z.-Y.; Li, G.; Zhang, Y. Investigation into optimization condition of thermal stimulation for hydrate dissociation in the sandy reservoir. *Appl. Energy* **2015**, *154*, 995–1003. [CrossRef]
20. Wu, P.; Li, Y.; Liu, W.; Liu, Y.; Wang, D.; Song, Y. Microstructure evolution of hydrate-bearing sands during thermal dissociation and ensued impacts on the mechanical and seepage characteristics. *J. Geophys. Res. Solid Earth* **2020**, *125*, e2019JB019103. [CrossRef]
21. Sun, Y.-F.; Zhong, J.-R.; Li, W.-Z.; Ma, Y.-M.; Li, R.; Zhu, T.; Ren, L.-L.; Chen, G.-J.; Sun, C.-Y. Methane recovery from hydrate-bearing sediments by the combination of ethylene glycol injection and depressurization. *Energy Fuels* **2018**, *32*, 7585–7594. [CrossRef]
22. Liang, M.; Gushchin, P.; Khlebnikov, V.; Antonov, S.; Mishin, A.; Khamidullina, I.; Likhacheva, N.; Semenov, A.; Vinokurov, V. Methane Recovery from Natural Gas Hydrate via CO 2/CH 4 Injection in the Presence of Methanol Aqueous Solution. *Shiyou Huagong Gaodeng Xuexiao Xuebao* **2018**, *31*, 61–66.
23. Li, G.; Wu, D.; Li, X.; Zhang, Y.; Lv, Q.; Wang, Y. Experimental investigation into the production behavior of methane hydrate under methanol injection in quartz sand. *Energy Fuels* **2017**, *31*, 5411–5418. [CrossRef]
24. Sun, Y.-F.; Wang, Y.-F.; Zhong, J.-R.; Li, W.-Z.; Li, R.; Cao, B.-J.; Kan, J.-Y.; Sun, C.-Y.; Chen, G.-J. Gas hydrate exploitation using CO2/H2 mixture gas by semi-continuous injection-production mode. *Appl. Energy* **2019**, *240*, 215–225. [CrossRef]
25. Xie, Y.; Zhu, Y.-J.; Zheng, T.; Yuan, Q.; Sun, C.-Y.; Yang, L.-Y.; Chen, G.-J. Replacement in CH4-CO2 hydrate below freezing point based on abnormal self-preservation differences of CH4 hydrate. *Chem. Eng. J.* **2021**, *403*, 126283. [CrossRef]
26. Veluswamy, H.P.; Kumar, A.; Seo, Y.; Lee, J.D.; Linga, P. A review of solidified natural gas (SNG) technology for gas storage via clathrate hydrates. *Appl. Energy* **2018**, *216*, 262–285. [CrossRef]
27. Yan, L.; Chen, G.; Pang, W.; Liu, J. Experimental and modeling study on hydrate formation in wet activated carbon. *J. Phys. Chem. B* **2005**, *109*, 6025–6030. [CrossRef]
28. Manakov, A.Y.; Stoporev, A. physical chemistry of gas hydrates and their technological application: State of the art. *Russ. Chem. Rev.* **2021**, *90*, 90. [CrossRef]
29. Oignet, J.; Hoang, H.M.; Osswald, V.; Delahaye, A.; Fournaison, L.; Haberschill, P. Experimental study of convective heat transfer coefficients of CO2 hydrate slurries in a secondary refrigeration loop. *Appl. Therm. Eng.* **2017**, *118*, 630–637. [CrossRef]
30. Misyura, S.Y.; Donskoy, I.G. Ways to improve the efficiency of carbon dioxide utilization and gas hydrate storage at low temperatures. *J. CO2 Util.* **2019**, *34*, 313–324. [CrossRef]
31. Khlebnikov, V.; Antonov, S.; Mishin, A.; Liang, M.; Khamidullina, I.; Zobov, P. The main influence factors of gas hydrate formation in porous media. *Nat. Gas Ind.* **2017**, *5*, 38–45.
32. Liu, H.; Zhan, S.; Guo, P.; Fan, S.; Zhang, S. Understanding the characteristic of methane hydrate equilibrium in materials and its potential application. *Chem. Eng. J.* **2018**, *349*, 775–781. [CrossRef]
33. Li, X.-Y.; Wang, Y.; Li, X.-S.; Zhang, Y.; Chen, Z.-Y. Experimental study of methane hydrate dissociation in porous media with different thermal conductivities. *Int. J. Heat Mass Transf.* **2019**, *144*, 118528. [CrossRef]
34. Bhattacharjee, G.; Kumar, A.; Sakpal, T.; Kumar, R. Carbon dioxide sequestration: Influence of porous media on hydrate formation kinetics. *ACS Sustain. Chem. Eng.* **2015**, *3*, 1205–1214. [CrossRef]
35. Zhang, Y.; Li, X.; Wang, Y.; Chen, Z.; Li, G. Methane hydrate formation in marine sediment from South China Sea with different water saturations. *Energies* **2017**, *10*, 561. [CrossRef]
36. Em, Y.; Stoporev, A.; Semenov, A.; Glotov, A.; Smirnova, E.; Villevald, G.; Vinokurov, V.; Manakov, A.; Lvov, Y. Methane Hydrate Formation in Halloysite Clay Nanotubes. *ACS Sustain. Chem. Eng.* **2020**, *8*, 7860–7868. [CrossRef]
37. Sun, Y.; Jiang, S.; Li, S.; Wang, X.; Peng, S. Hydrate formation from clay bound water for CO2 storage. *Chem. Eng. J.* **2021**, *406*, 126872. [CrossRef]
38. Linga, P.; Daraboina, N.; Ripmeester, J.A.; Englezos, P. Enhanced rate of gas hydrate formation in a fixed bed column filled with sand compared to a stirred vessel. *Chem. Eng. Sci.* **2012**, *68*, 617–623. [CrossRef]
39. Dai, S.; Lee, J.Y.; Santamarina, J.C. Hydrate nucleation in quiescent and dynamic conditions. *Fluid Phase Equilibria* **2014**, *378*, 107–112. [CrossRef]
40. Zhang, L.; Sun, M.; Sun, L.; Yu, T.; Song, Y.; Zhao, J.; Yang, L.; Dong, H. In-situ observation for natural gas hydrate in porous medium: Water performance and formation characteristic. *Magn. Reson. Imaging* **2020**, *65*, 166–174. [CrossRef]
41. Benmesbah, F.D.; Ruffine, L.; Clain, P.; Osswald, V.; Fandino, O.; Fournaison, L.; Delahaye, A. Methane Hydrate Formation and Dissociation in Sand Media: Effect of Water Saturation, Gas Flowrate and Particle Size. *Energies* **2020**, *13*, 5200. [CrossRef]
42. Sun, S.-C.; Liu, C.-L.; Ye, Y.-G.; Liu, Y.-F. Phase behavior of methane hydrate in silica sand. *J. Chem. Thermodyn.* **2014**, *69*, 118–124. [CrossRef]
43. Bagherzadeh, S.A.; Moudrakovski, I.L.; Ripmeester, J.A.; Englezos, P. Magnetic Resonance Imaging of Gas Hydrate Formation in a Bed of Silica Sand Particles. *Energy Fuels* **2011**, *25*, 3083–3092. [CrossRef]
44. Liu, C.; Lu, H.; Ye, Y.; Ripmeester, J.A.; Zhang, X. Raman spectroscopic observations on the structural characteristics and dissociation behavior of methane hydrate synthesized in silica sands with various sizes. *Energy Fuels* **2008**, *22*, 3986–3988. [CrossRef]
45. Pan, Z.; Liu, Z.; Zhang, Z.; Shang, L.; Ma, S. Effect of silica sand size and saturation on methane hydrate formation in the presence of SDS. *J. Nat. Gas Sci. Eng.* **2018**, *56*, 266–280. [CrossRef]

46. Chen, Q.; Liu, C.L.; Ye, Y.G. Differential Scanning Calorimetry Research of Hydrates Phase Equilibrium in Porous Media. *Adv. Mater. Res.* **2012**, *512–515*, 2122–2126. [CrossRef]
47. Xie, Y.; Zheng, T.; Zhong, J.-R.; Zhu, Y.-J.; Wang, Y.-F.; Zhang, Y.; Li, R.; Yuan, Q.; Sun, C.-Y.; Chen, G.-J. Experimental research on self-preservation effect of methane hydrate in porous sediments. *Appl. Energy* **2020**, *268*, 115008. [CrossRef]
48. Dalmazzone, C.; Dalmazzone, D.; Herzhaft, B. Differential scanning calorimetry: a new technique to characterize hydrate formation in drilling muds. In Proceedings of the SPE Annual Technical Conference and Exhibition, Dallas, TX, USA, 1–4 October 2000.
49. Youssef, S.; Rosenberg, E.; Gland, N.F.; Kenter, J.A.; Skalinski, M.; Vizika, O. High resolution CT and pore-network models to assess petrophysical properties of homogeneous and heterogeneous carbonates. In Proceedings of the SPE/EAGE Reservoir Characterization and Simulation Conference, Abu Dhabi, UAE, 28–31 October 2007.
50. Maeda, N. Interfacial Nanobubbles and the Memory Effect of Natural Gas Hydrates. *J. Phys. Chem. C* **2018**, *122*, 11399–11406. [CrossRef]
51. Holzammer, C.; Schicks, J.M.; Will, S.; Braeuer, A.S. Influence of Sodium Chloride on the Formation and Dissociation Behavior of CO2 Gas Hydrates. *J. Phys. Chem. B* **2017**, *121*, 8330–8337. [CrossRef]
52. Fukumoto, A.; Kamada, K.; Sato, T.; Oyama, H.; Torii, H.; Kiyono, F.; Nagao, J.; Temma, N.; Narita, H. Numerical simulation of pore-scale formation of methane hydrate in the sand sediment using the phase-field model. *J. Nat. Gas Sci. Eng.* **2018**, *50*, 269–281. [CrossRef]
53. Stoporev, A.S.; Svarovskaya, L.I.; Strelets, L.A.; Altunina, L.K.; Villevald, G.V.; Karpova, T.D.; Rodionova, T.V.; Manakov, A.Y. Nucleation of methane hydrate and ice in emulsions of water in crude oils and decane under non-isothermal conditions. *Chin. J. Chem. Eng.* **2019**, *27*, 668–676. [CrossRef]
54. Qin, J.; Kuhs, W.F. Quantitative analysis of gas hydrates using Raman spectroscopy. *AIChE J.* **2013**, *59*, 2155–2167. [CrossRef]